Removal of NO_x and NO_y in Asian outflow plumes: Aircraft measurements over the western Pacific in January 2002

N. Takegawa,[1] Y. Kondo,[1] M. Koike,[2] G. Chen,[3] T. Machida,[4] T. Watai,[5] D. R. Blake,[6] D. G. Streets,[7] J.-H. Woo,[8] G. R. Carmichael,[8] K. Kita,[9] Y. Miyazaki,[1] T. Shirai,[10] J. B. Liley,[11] and T. Ogawa[10]

1. Research Center for Advanced Science and Technology, University of Tokyo, Tokyo, Japan.
2. Department of Earth and Planetary Science, University of Tokyo, Tokyo, Japan.
3. NASA Langley Research Center, Hampton, VA, USA.
4. National Institute for Environmental Studies, Ibaraki, Japan.
5. Global Environmental Forum, Ibaraki, Japan.
6. Department of Chemistry, University of California, Irvine, CA, USA.
7. Decision and Information Sciences Division, Argonne National Laboratory, IL, USA.
8. Center for Global and Regional Environmental Research, University of Iowa, IA, USA.
9. Department of Environmental Science, Ibaraki University, Ibaraki, Japan.
10. Earth Observation Research and Application Center, Japan Aerospace Exploration Agency, Tokyo, Japan.
11. National Institute of Water and Atmospheric Research, Lauder, New Zealand.

Short title: REMOVAL OF NOX AND NOY

Submitted to JGR-Atmospheres (ITCT-2K2/PEACE special section)

April 5, 2004

Abstract. The Pacific Exploration of Asian Continental Emission Phase A (PEACE-A) aircraft measurement campaign was conducted over the western Pacific in January 2002. Correlations of carbon monoxide (CO) with carbon dioxide (CO_2) and back trajectories are used to identify plumes strongly affected by Asian continental emissions. $\Delta CO/\Delta CO_2$ ratios (i.e., linear regression slopes of CO-CO_2) in the plumes generally fall within the variability range of the CO/CO_2 emission ratios estimated from an emission inventory for East Asia, demonstrating the consistency between the aircraft measurements and the emission characterization. Removal rates of reactive nitrogen (NO_x and NO_y) for the study region (c.a., altitude < 4 km, 124°-140°E, 25°-45°N) are estimated using correlation with CO_2, the photochemical age of the plumes, and the NO_x/CO_2 emission ratio derived from the emission inventory. The plume age is estimated from the rates of hydrocarbon decay and hydroxyl radical (OH) concentration calculated using a constrained photochemical box model. The average lifetime of NO_x is estimated to be 1.2 ± 0.4 days. Possible processes controlling the NO_x lifetime are discussed in conjunction with results from earlier studies. The average lifetime of NO_y is estimated to be 1.7 ± 0.5 days, which is comparable to the NO_y lifetime of 1.7-1.8 days that has previously been reported for outflow from the United States. This similarity suggests the

importance of chemical processing near the source regions in determining the NO_y budget.

1. Introduction

Fossil fuel combustion and biomass burning in East Asia are large sources of trace gases such as carbon monoxide (CO), carbon dioxide (CO_2), nitrogen oxides (NO_x), sulfur dioxide (SO_2), and volatile organic compounds (VOCs) [*Streets et al.*, 2003]. These emissions can significantly affect the distribution of ozone (O_3) over the western Pacific, and even the United States by long-range intercontinental transport [*Jaffe et al.*, 2003]. To assess the impact of Asian emissions on O_3 and its precursors on regional/hemispheric scales, it is important to evaluate the loss rate of reactive nitrogen species (NO_x and NO_y) during transport processes, because these species are the most critical in determining O_3 concentrations.

A number of aircraft /ground-based measurements have been conducted in East Asia to investigate the chemical characteristics of Asian outflow. The NASA Pacific Exploratory Mission - West campaigns (PEM-West A: September-October 1991; PEM-West B: February-March 1994) were the first systematic studies focusing on the impact of Asian outflow over the western Pacific [*Hoel et al.*, 1996, 1997]. The NASA Transport and Chemical Evolution over the Pacific (TRACE-P) mission was conducted in the same region in February-April 2001, deploying improved instrumentation and using three-dimensional chemical transport models (3D-CTMs) [*Jacob et al.*, 2003].

The Pacific Exploration of Asian Continental Emission (PEACE) aircraft measurement campaign was designed to investigate the chemical characteristics of Asian outflow over the western Pacific in winter and late spring. These seasons have not been covered by PEM-West-B and TRACE-P [*Kondo et al.*, this issue]. The PEACE campaign consists of two phases (phase A: January 2002; phase B: April-May 2002). In this analysis we focus on the data obtained during the PEACE-A campaign. The major purpose of this paper is to estimate the removal rates of NO_x and NO_y. A brief description of the aircraft measurements during PEACE-A is given in section 2. An emission inventory for East Asia in January 2002 is described in section 3. We use CO and CO_2 as tracers of Asian outflow, and the method of our analysis is described in section 4. A comparison of the observations with the emission inventory and estimates of the removal rates of NO_x and NO_y are presented in section 5.

2. Aircraft Measurements

2.1. Airborne Instruments

In situ measurements of gases and aerosols were made onboard the Gulfstream-II (G-II) aircraft. The instruments used for the

PEACE-A campaign were similar to those used for the Biomass Burning and Lightning Experiment Phase B (BIBLE-B) campaign [*Kondo et al*., 2002]. A brief description of the key measurements in this analysis is given below. CO mixing ratios were measured using a vacuum ultraviolet (VUV) resonance fluorescence technique with a time resolution of 1 s [*Takegawa et al*., 2001]. CO_2 was measured using a non-dispersive infrared absorption (NDIR) technique with a time resolution of 1 s (LI-COR) [*Machida et al*., 2002]. Measurements of non-methane hydrocarbons (NMHCs) were made using a whole air sampling technique followed by laboratory analysis [*Blake et al*., 2003]. The integration time of the whole air sampling was typically 40-60 s at lower altitudes (< 4 km).

Nitric oxide (NO) and total reactive nitrogen (NO_y) were measured using a NO-O_3 chemiluminescence detector with a time resolution of 1 s [*Kondo et al*., 1997, 2004]. Photostationary NO_2 mixing ratios were calculated using a photochemical box model and the sum of observed NO and calculated NO_2 is given as NO_x. NO_y compounds were catalytically converted to NO on the surface of a gold tube heated at 300°C. The effect of particulate nitrate (NO_3^-) on the NO_y measurements is evaluated here. During PEACE-A, two converter systems were placed in the aircraft pod and were connected to two independent inlets: one directed forward and the other rearward. NO_y measurements made using the forward-facing inlet are referred to as NO_y(f) and those using the rearward-facing inlet as NO_y(r). Our recent studies have shown that the NO_y(r) represents the sum of gas-phase NO_y and submicron non-refractory NO_3^- aerosols [*Kondo et al.*, 2004]. Note that non-refractory means volatile at 300°C (e.g., NH_4NO_3). We define supermicron non-refractory NO_3^- as

$$\text{Supermicron non-refractory } NO_3^- = (NO_y(f) - NO_y(r))/EF, \qquad (1)$$

where EF (~50 at a particle diameter of 1 μm) represents the enhancement factor for the forward-facing inlet due to sub-isokinetic sampling. For the entire dataset used in this analysis we found that the supermicron non-refractory NO_3^- was negligibly small as compared to NO_y(r), indicating that the majority of non-refractory NO_3^- in the ambient air was distributed in the submicron mode during PEACE-A. Hereafter NO_y(r) is expressed simply as NO_y and is used for the present analysis. Therefore, the term "removal of NO_y" in this analysis represents either dry/wet deposition of NO_y compounds or conversion of NO_y compounds to refractory NO_3^- aerosols (e.g., $Ca(NO_3)_2$, $NaNO_3$). Because such conversion is generally an irreversible process, it can be regarded as an ultimate sink of NO_y in the atmosphere.

2.2. Vertical Profiles

Figure 1 shows the flight tracks of the G-II aircraft during the PEACE-A campaign. Thirteen flights were conducted, mainly over the Sea of Japan (35°-45°N) and the East China Sea (20°-35°N) during January 6-23, 2002. Figure 2 shows an example of vertical profiles of CO, CO_2, NO_x, NO_y, O_3, and relative humidity (RH) observed over the Sea of Japan (132°E, 36°N) on January 11, 2002 (flight 04). Large enhancements of CO mixing ratios (200-400 parts per billion by volume (ppbv)) were observed below 2.5 km. The CO mixing ratios between 2.5 and 4 km were relatively high (100-200 ppbv), while those above 4 km were fairly constant at ~100 ppbv. Correspondingly, the RH profile showed a slight decrease at 2.5 km and a sharp gradient at 4 km. The former is interpreted as the top of the convective boundary layer where the air masses were well mixed, and the latter as the top of the planetary boundary layer where the air masses had been influenced by surface emissions but not well mixed. The CO_2 and NO_y profiles exhibit almost the same vertical structures as the CO profile. There is no clear structure in the O_3 profile, although O_3 seems to have a weak positive correlation with CO (< 1 km). A detailed analysis of the O_3 production and loss rates during PEACE-A is presented by *Kondo et al.* [this issue].

Profiles similar to Figure 2 were frequently observed during PEACE-A, and we rarely found significant enhancements of primary emissions such as CO, CO_2, and NO_y above 4 km. Reanalysis data from the National Centers for Environmental Prediction (NCEP) (http://www.ncep.noaa.gov/) indicate that air flow patterns in the boundary layer over East Asia were strongly influenced by the Siberian High in January 2002. It is likely that the vertical transport of trace gases was not effective during PEACE-A because of the strong influence of the Siberian High during this period.

3. Emission Inventory

3.1. Distribution of CO/CO_2 Emission Ratio

A comprehensive emission inventory of gaseous and particulate emissions in East Asia for the year 2000 has been developed by *Streets et al*. [2003] and evaluated by several investigators using 3-D CTMs [e.g., *Palmer et al*., 2003; *Woo et al*., 2003]. *Streets et al*. [2003] showed that the emissions of CO, CO_2, and other species from the Asian continent tend to have an annual maximum in January mainly due to an increase in domestic heating. An emission inventory for January 2002 was produced for this study taking into account the seasonal trends of gaseous and particulate emissions [*Streets et al*., 2003] and assuming that the annually averaged anthropogenic emissions in 2002 were the same as those in 2000. Figure 3 shows a 1° x 1° grid distribution of CO/CO_2 emission ratios for January 2002. Although the emission inventory includes both anthropogenic and biomass burning sources, major primary emissions such as CO, CO_2, and NO_x were likely dominated by anthropogenic sources because the biomass burning activities in East Asia were very weak in January 2002 (e.g., from fire images from the Along Track Scanning Radiometer (ATSR) (http://shark1.esrin.esa.it/ionia/FIRE/AF/ATSR/)).

Emission ratios for CO/CO_2 have been used as a good proxy for evaluating the combustion efficiency of emission sources, especially for biomass burning studies [e.g., *Yokelson et al*., 2003]. Lower CO/CO_2 emission ratios correspond to higher combustion efficiency. Because combustion efficiency strongly depends on fuel type (petroleum, coal, etc.) and devices (engine, furnace, etc.), CO/CO_2 emission ratios can be used for diagnosing the types of emission sources. For example, low CO/CO_2 emission ratios (< 0.02) typically originate from combustion of well-processed gas/liquid fuels (vehicular engines, natural gas stoves, etc.) [e.g., *Zhang et al*., 2000]. By contrast, high CO/CO_2 emission ratios (0.03-0.1) typically come from combustion of poorly processed solid fuels (coal/biofuel stoves, biomass burning, etc.) [e.g., *Yokelson et al*., 2003; *Zhang et al*., 2000]. Fossil fuel power plants, ship engines, and aircraft engines generally have extremely high combustion efficiencies, producing much less CO relative to CO_2 as compared to other sources [e.g., *Nicks, et al*., 2003]. Figure 3 clearly illustrates that the emissions from Japan and South Korea are dominated by high-combustion efficiency sources, while those from China are dominated by relatively low-combustion efficiency sources.

3.2. Definition of Source Regions

We have classified the source regions into four categories as follows: Japan (mainly Nagoya) (136°-138°E, 34°-36°N), Korea (mainly Pusan) (126°-130°E, 34°-36°N), Northern China (110°-125°E, 35°-44°N), and Central China (105°-123°E, 26°-35°N) (Figure 3). The emission ratios of Y to X (X, Y = CO, CO_2, NO_x, etc.) for the individual source regions were calculated as follows and are summarized in Table 1.

$$E_{Y\text{-}X} = \frac{\sum_i F_Y^i}{\sum_i F_X^i} \quad (i = 0,1, \ldots) \tag{2}$$

$$E_{Y-X}^{Max} = \text{Maximum value of } F_Y^i / F_X^i \tag{3}$$

$$E_{Y-X}^{Min} = \text{Minimum value of } F_Y^i / F_X^i \tag{4}$$

$E_{Y\text{-}X}$, E_{Y-X}^{Max}, E_{Y-X}^{Min} are the average, maximum, and minimum values of the Y to X emission ratio, respectively. F_X^i and F_Y^i are the emission rates (mol month^{-1} grid^{-1}) of species X and Y for the i-th grid box in the individual source region, respectively. Only data with

$F^{i}_{CO} > 0.2$ Gmol month^{-1} grid^{-1} were used to determine the values of E^{Max}_{Y-X} and E^{Min}_{Y-X} because the variations of F^{i}_{Y} / F^{i}_{X} for small emission sources may not be representative. It should be noted that the uncertainties in the emission rates are not taken into account in determining the maximum and minimum values: CO (156% for China, 34% for Japan, and 84% for other East Asia), CO_2 (16% for China, 7% for Japan, and 13% for other East Asia), NO_x (23% for China, 19% for Japan, and 24% for other East Asia) [*Streets et al.*, 2003].

As described in section 3.1, emissions from Japan (Nagoya) and Korea (Pusan) are dominated by high-combustion efficiency sources (low CO/CO_2), while those from Northern/Central China are dominated by low-combustion efficiency sources (high CO/CO_2). Details about the interpretation of NO_x/CO and NO_x/CO_2 emission ratios are given in section 5.1.2. Note that the ethene (C_2H_4) to ethyne (C_2H_2) emission ratios are specifically listed in Table 1 because these species are used to estimate the photochemical age of air masses (section 5.2).

4. Method of Analysis

4.1. Definition of Plumes

The major purpose of this paper is to estimate the removal rates of NO_x and NO_y in Asian outflow during PEACE-A. To achieve this goal, we first need to identify air masses that were strongly affected by Asian continental emissions. The Y to X enhancement ratio relative to regional background air (ΔY/ΔX ratio), defined by the linear regression slope of Y-X correlation, is used for the air mass identification. The regional background air represents relatively clean air that dilutes polluted air masses emitted from anthropogenic sources. Ten-day back trajectories were calculated for the sampled air masses using meteorological data with a horizontal resolution of 1° in longitude and 1° in latitude. The data were provided by the European Centre for Medium-Range Weather Forecasts (ECMWF) (http://www.ecmwf.int). In this analysis, "plume" is defined as air masses that meet the following three criteria (a)-(c).

(a) The air masses were sampled below 4 km, and the back trajectories for the air masses had passed over one of the source regions defined in section 3.2.

(b) The enhancement of CO (ΔCO) in the air masses is larger than 50 ppbv, and that of CO_2 (ΔCO_2) is larger than 5 parts per million by volume (ppmv).

(c) The square of the linear correlation coefficient (r^2) for the CO-CO_2 correlation is larger than 0.7.

The threshold values (ΔCO = 50 ppbv, ΔCO_2 = 5 ppmv, and r^2 = 0.7) were determined rather arbitrarily. The identified plumes are summarized in Table 2. The plume ID consists of a group name (e.g., Japan-1, Korea-1, N-China-1, and C-China-1), a flight number (F01, F02, etc.), and a leg number (L01, L02, etc.). First, the duration of each flight was divided into 5-14 flight legs based on sampling altitudes and back trajectories. Second, the source region for each leg was investigated using the trajectories, and the group name was determined corresponding to Table 1. Note that different flight numbers and legs with similar sampling locations on the same day belong to the same group (e.g., both F02L08 and F02L12 belong to Korea-1) but are treated as different plumes. A comparison of the observed $\Delta CO/\Delta CO_2$ ratios to the CO/CO_2 emission ratios estimated from the emission inventory is discussed in section 5.1.1.

The majority of the plumes were sampled below 3 km because the vertical transport was weak during PEACE-A (section 2.2). The infrequent vertical mixing of air masses during the PEACE-A period should have caused the accumulation of pollutants at lower altitudes, leading to the formation of distinct plumes. Indeed, we rarely found such distinct plumes in the same altitude regime during the PEACE-B period (April-May, 2002), when the upward lifting by convection was very active over central China [*Oshima et al.*, this issue].

4.2. Interpretation of ΔY/ΔX Ratio

Trajectory analysis shows that the transport time from source regions to sampling points was generally less than 4 days. Therefore, chemical species with photochemical lifetimes longer than 1 month (>> 4 days) can be regarded as long-lived, and those with photochemical lifetimes shorter than ~4 days as short-lived. Table 3 summarizes the photochemical lifetimes of CO and NMHCs against reactions with OH under the conditions experienced during PEACE-A. The diurnally averaged OH concentrations were calculated using a constrained photochemical box model. The data obtained below 3 km were used to calculate the median OH concentration because the majority of the plumes were transported below 3 km prior to the measurements. The median value (+/- 67% range) of OH concentration was 5 (+6/-3) $\times 10^5$ cm^{-3}. The kinetic parameters listed by *Atkinson et al*. [1992] and *Calvert et al.* [2000] were used for calculating the rates of OH reactions. In Table 3, CO, ethane (C_2H_6), and C_2H_2 correspond to long-lived species, and C_2H_4 and propene (C_3H_6) correspond to short-lived species.

If X and Y are both long-lived, the $\Delta Y/\Delta X$ ratio should be equal to the $E_{Y\text{-}X}$ (or between E^{Max}_{Y-X} and E^{Min}_{Y-X}) of the source region estimated from the trajectories.

$$\Delta Y/\Delta X = E_{Y\text{-}X} \quad \text{(X, Y: long-lived)} \qquad (5)$$

If X is a long-lived species and Y is a short-lived species, the $\Delta Y/\Delta X$ ratio should be systematically smaller than $E_{Y\text{-}X}$ because of the removal (including both photochemical loss and deposition) of species Y. In this case, we assume that the $\Delta Y/\Delta X$ ratio is approximated as:

$$\Delta Y/\Delta X = E_{Y\text{-}X} \exp(-\, t/\tau_Y) \quad \text{(X: long-lived; Y: short-lived),} \qquad (6)$$

where t and τ_Y are the elapsed time since emission and the photochemical lifetime of species Y, respectively.

Strictly speaking, $\Delta Y/\Delta X$ ratios are affected by chemical and dilution processes, and these two effects are generally not distinguishable [*McKeen et al*., 1996; *Takegawa et al*., 2003]. However, we can use the equation (6) under the conditions where the mixing ratio of Y in the background air is much smaller than that in the plume. This condition is applicable to the short-lived species considered in this analysis (i.e., Y = NO_x, NO_y, C_2H_4).

5. Results and Discussion

5.1. Comparison of Observations with Emission Inventory

5.1.1. CO/CO_2 emission ratio

The $\Delta CO/\Delta CO_2$ ratios observed in the plumes can be directly compared to the CO/CO_2 emission ratios from the source regions because the production and loss of CO during transport should be negligible on a time scale of ~4 days. We consider that biogenic sources/sinks of CO_2 such as vegetation did not significantly affect the $\Delta CO/\Delta CO_2$ ratios for this analysis because of the following two reasons. First, gross flux of CO_2 from/to vegetation is likely small during the PEACE-A period because biogenic activity is weak in winter. Second, we have chosen distinct plumes in which the enhancements of CO_2 are large (> 5 ppmv) and the correlation of CO versus CO_2 is tight ($r^2 > 0.7$). Vegetation is generally distributed over a wide area as compared to the anthropogenic sources. Thus, it should affect the CO_2 mixing ratios in regional background air (i.e., air masses that dilute the plumes) rather than in the formation of such distinct plumes. Although CO_2 mixing ratios in regional background air sometimes show vertical structures, the variability range is typically less than 1 ppmv [*Machida et al*., 2003].

Figure 4 shows correlations of CO versus CO_2 for all of the plumes listed in Table 2. The most important feature is that the observed $\Delta CO/\Delta CO_2$ ratios exhibit distinct values depending on the source region, indicating that they can be used as a good tracer for investigating the origins of anthropogenic plumes. In addition, the observed $\Delta CO/\Delta CO_2$ ratio falls within the variability range of the CO/CO_2 emission ratio for most of the plumes, demonstrating the overall consistency among the aircraft measurements, trajectories, and emission characterization.

Examples of individual plumes are shown in Figures 5 and 6 (Korea-1 (F02L08) and N-China-1 (F04L02) plumes in Table 2, respectively). These figures include time series of CO mixing ratios, back trajectories, and CO-CO_2 correlations for the plumes. Note that the ratio of vertical to horizontal scales is the same as that in Figure 4 so that one can readily see the similarities and differences in the slopes. The $\Delta CO/\Delta CO_2$ ratio observed in the Korea-1 (F02L08) plume was higher by ~25% than the average CO/CO_2 emission ratio from the Korea region. On the other hand, the $\Delta CO/\Delta CO_2$ ratio observed in the N-China-1 (F04L02) plume was lower by ~30% than the average CO/CO_2 emission ratio from the Northern China region. A similar tendency is found for the other plumes (Table 2). However, these small discrepancies may not be significant when we take into account the variability range (i.e., minimum and maximum values) of the CO/CO_2 emission ratios and the uncertainties in the emission rates for CO and CO_2 (see section 3.2).

Correlations of halocarbons with CO can provide additional information on the chemical characteristics of the plumes. Figures 7 and 8 depict the correlations of methyl bromide (CH_3Br) and Halon-1211 (H-1211) with CO in the Korea-1 (F02L08) and N-China-1 (F04L02) plumes, respectively (same plumes as Figures 5 and 6). *Blake et al.* [2003] found that CH_3Br is a good tracer of Japan and Korea emissions and H-1211 is a good tracer of China emissions, based on the whole air samples collected during the TRACE-P campaign. The Korea plume shows a higher $\Delta CH_3Br/\Delta CO$ ratio and lower Δ(H-1211)/ΔCO ratio than the Northern China plume, which is consistent with the findings of *Blake et al.* [2003].

5.1.2. NO_x/CO and NO_x/CO_2 emission ratios

Two fresh plumes were sampled below 1.5 km over Nagoya, Japan on January 7 and 10, 2002 (Japan-2 (F02L14) and Japan-4 (F03L08) plumes in Table 2). Figures 9a-9b show the correlations of NO_y with CO and CO_2 in the plumes. Assuming that loss of NO_y in these fresh plumes was negligible, the $\Delta NO_y/\Delta CO$ (or $\Delta NO_y/\Delta CO_2$) ratios for these plumes can be interpreted as the NO_x/CO (or NO_x/CO_2) emission ratios for this region. The observed $\Delta NO_y/\Delta CO$ ratios were lower by a factor of ~2 than the average NO_x/CO emission ratio estimated from the emission inventory (Figure 9a). The discrepancy is still significant even though we take into account the variability range (i.e., minimum and maximum values) of the NO_x/CO emission ratio and the uncertainties in the emission rates for NO_x and CO. By contrast, the observed $\Delta NO_y/\Delta CO_2$ ratios showed good agreement with the emission inventory (Figure 9b).

For comparison, we show data observed in fresh savanna fire plumes over northern Australia during the BIBLE-B campaign [*Shirai et al.*, 2003; *Takegawa et al.*, 2003]. The $\Delta CO/\Delta CO_2$, $\Delta NO_y/\Delta CO$, and $\Delta NO_y/\Delta CO_2$ ratios observed in fresh savanna fire plumes were 86 ppbv/ppmv, 0.018 ppbv/ppbv, and 1.5 ppbv/ppmv, respectively. There is a significant difference in the $\Delta NO_y/\Delta CO$ ratios between Nagoya (PEACE-A) and Australia (BIBLE-B), while the $\Delta NO_y/\Delta CO_2$ ratios are comparable. It has been pointed out that the NO_x/CO_2 emission ratios from biomass burning are relatively uniform (2 ± 1 ppbv/ppmv) for various types of fires, although they have a dependence on the nitrogen content of the fuels [*Andreae et al.*, 1994; *Yokelson et al.*, 2003; and references therein]. The results obtained in this study suggest that the uniformity of NO_x/CO_2 emission ratios holds even though the types of emission sources are significantly different from biomass burning.

The preceding discussion provides some insights into the merits and disadvantages of using CO or CO_2 as a tracer of NO_x from combustion sources. CO_2 is a good tracer for NO_x because these two species are major products of high combustion efficiency processes, while biogenic interactions of CO_2 sometimes make it difficult to define the signals from combustion sources, especially for aged air masses. CO does not have interactions with biogenic sources/sinks, while NO_x/CO emission ratios show a large variability depending on the combustion efficiency, especially for the cases where the emission sources are heterogeneous. In addition, the uncertainty in the emission rate of CO is much larger than that of CO_2, as described in section 3.2. In the present analysis we have chosen only distinct plumes where the enhancements of CO_2 are large (> 5 ppmv) and the correlation of CO versus CO_2 is tight ($r^2 > 0.7$). Therefore, we choose CO_2 as a tracer of NO_x rather than CO to estimate the removal rates of NO_x and NO_y.

5.2. Plume Age Derived from Hydrocarbons

The elapsed time since emission for each plume (plume age) can be estimated using equation (6) and ratios of NMHCs with known photochemical lifetimes (Table 3). We define plume age (t) as follows:

$$t = \overline{\tau_{C2H4}} \; [\ \ln(E_{C2H4\text{-}C2H2}) - \ln(\Delta C_2H_4/\Delta C_2H_2)\ ], \qquad (7)$$

where $\overline{\tau_{C2H4}}$ (= 2.7 days) is the average lifetime of C_2H_4 during PEACE-A (Table 3). The uncertainty in the plume age was estimated from the fitting error for the $\Delta C_2H_4/\Delta C_2H_2$ ratio and the maximum and minimum values of the emission ratio given by equations (3) and (4). Note that the plume age is not very sensitive to the uncertainty in the emission ratio because it is proportional to the logarithm of the ratio. The uncertainty in the photochemical lifetime of C_2H_4 is not included. We have chosen C_2H_2 as a long-lived species and C_2H_4 as a short-lived species because of the following two reasons. First, the lifetime of C_2H_4 is 2.7 days so that the photochemical history of the plumes (typically < 4 days old) can be clearly resolved. Second, the emission ratio of C_2H_4 to C_2H_2 ($E_{C2H4-C2H2}$) does not significantly depend on the type of emission source (Table 1). The uniformity of C_2H_4/C_2H_2 emission ratio is understandable considering the similarity in the emission patterns of these two species, which are dominated by biofuel burning and transportation for East Asia [*Streets et al.*, 2003, Figure 6].

The plume age estimated for each plume is shown in Table 4. The number of plumes is smaller than that in Table 2 because it is limited by the availability of NMHC data. For comparison, transport time was roughly estimated based on the trajectories and is listed in Table 4. The transport time tends to be shorter than the plume age for each plume. There are two possible explanations for this discrepancy. First, the transport time does not include the residence time (stagnant time) near the source region. Second, the plume age might be overestimated if OH concentrations in the plumes were actually higher than the median value of the model-predicted OH concentration (5×10^5 cm^{-3}), especially near the source regions. Indeed, earlier studies have shown that OH concentrations in fresh biomass burning or ship plumes were significantly higher than those in background air [*Hobbs et al.*, 2003; *Song et al.*, 2003]. Without detailed information on the OH chemistry in the plumes for this analysis, however, we use the median value of the model-predicted OH concentration to estimate the plume age.

5.3. Removal Rates of NO_x and NO_y

Figures 10 and 11 depict the correlations of NO_x and NO_y with CO_2 in the Korea-1 (F02L08) and N-China-1 (F04L02) plumes, respectively (same plumes as Figures 5 and 6). For both plumes, the $\Delta NO_x/\Delta CO_2$ and $\Delta NO_y/\Delta CO_2$ ratios are significantly lower than the NO_x/CO_2 emission ratios, indicating that removal of NO_x and NO_y occurred within the source region or during the transport from it. From equation (6) we obtain

$$(\Delta NO_x/\Delta CO_2)/E_{NOx\text{-}CO2} = \exp(-t/\tau_{NOx}) \quad (8)$$

$$(\Delta NO_y/\Delta CO_2)/E_{NOx\text{-}CO2} = \exp(-t/\tau_{NOy}) \quad (9)$$

The left hand sides of these equations give the fractions of NO_x and NO_y remaining in the observed plumes. Figures 12a and 12b depict the $(\Delta NO_x/\Delta CO_2)/E_{NOx\text{-}CO2}$ and $(\Delta NO_y/\Delta CO_2)/E_{NOx\text{-}CO2}$ as a function of the plume age (t) defined by equation (7), respectively. Each data point corresponds to the linear regression slope for each plume and is colored based on average sampling altitude. It should be noted that the photochemical age is assumed to be zero for the plumes sampled in the boundary layer over Nagoya, Japan because these plumes are considered to be very fresh (section 5.1.2). The uncertainty was estimated from fitting errors for the $\Delta NO_x/\Delta CO_2$ (or $\Delta NO_y/\Delta CO_2$) ratio and the maximum and minimum values of the NO_x to CO_2 emission ratios (Table 1). It is important to note that these plots do not represent a Lagrangian history for a particular event because the plumes were sampled at various locations on various days during PEACE-A. In spite of this variability, there is a clear tendency that both $(\Delta NO_x/\Delta CO_2)/E_{NOx\text{-}CO2}$ and $(\Delta NO_y/\Delta CO_2)/E_{NOx\text{-}CO2}$ show systematic decrease with plume aging. The plumes sampled at higher altitudes tend to exhibit older photochemical ages, probably because vertical transport was slow during PEACE-A.

The lifetimes of NO_x (τ_{NOx}) and NO_y (τ_{NOy}) for the individual plumes were estimated using equations (7), (8) and (9) (Table 4). The average lifetimes of NO_x ($\overline{\tau_{NOx}}$) and NO_y ($\overline{\tau_{NOy}}$) were 1.2 ± 0.4 and 1.7 ± 0.5 days, respectively. The errors were determined from the standard deviation (1-σ) of the average, and the uncertainty in the OH concentration (a factor of 2) was not taken into account for the error estimate. Alternative way for estimating $\overline{\tau_{NOx}}$ and $\overline{\tau_{NOy}}$ is to calculate linear regression slopes for the data points of Figures 12a and 12b. They were estimated as $\overline{\tau_{NOx}}$ = 1.1 ± 0.3 days and $\overline{\tau_{NOy}}$ = 1.6 ± 0.3 days, which are close to the values shown above. The errors were determined from 1-σ for the least squares fit.

The $(\Delta NO_y/\Delta CO_2)/E_{NOx\text{-}CO2}$ values shown in Table 4 indicate that 80-90% of NO_y was removed within 4 days following emission. The removal processes should be either dry or wet deposition of NO_y compounds, although quantitative estimates of the contributions from dry and wet deposition are difficult to achieve in this study. Assuming that dry/wet deposition of NO_x and peroxyacetyl nitrate (PAN) was negligible under PEACE-A conditions, this result suggests that the majority (> 80-90%) of NO_x emitted from surface sources was oxidized to HNO_3 or nitrate and a rapid removal of these species occurred in the plumes.

To obtain a better understanding of the behavior of NO_x oxidation products, the average NO_x/NO_y ratios and $(\Delta NO_z/\Delta CO_2)/E_{NOx\text{-}CO2}$ values in the plumes are plotted as a function of plume age (Figures 13a and 13b), where NO_z (=NO_y – NO_x) represents the NO_x oxidation products. The $(\Delta NO_z/\Delta CO_2)/E_{NOx\text{-}CO2}$ values represent the fraction of NO_z produced per NO_x emitted (i.e., NO_z yield). The NO_z yield would eventually approach 100% if there were no removal of NO_z. However, it exhibited a broad maximum (10-15%) at plume ages of 2-3 days and then decreased with air mass aging after 3 days. Although this tendency does not represent a Lagrangian history for a particular event as mentioned earlier, it may be interpreted as follows. The NO_z yield showed a net increase at plume ages of < 2 days because the oxidation rate of NO_x was faster than the removal rate of NO_z. After 3 days when the NO_x/NO_y ratio decreased to as low as 10%, the oxidation of NO_x was not an effective source of NO_z any more, and the NO_z yield showed a net decrease with air mass aging.

5.3.1. Interpretation of NO_x lifetime

Here we investigate whether the estimated NO_x loss rates in the plumes can be explained by the conversion of NO_x to HNO_3 and nitrate. Detailed investigation is, however, somewhat speculative due to the lack of in situ measurements of NO_x reservoirs such as HNO_3, nitrate, and PAN during PEACE-A. NO_x is oxidized to HNO_3 by reaction of NO_2 with OH during the daytime,

$$NO_2 + OH + M \rightarrow HNO_3 + M \qquad \text{(R1)}$$

During the nighttime, NO_3 formation followed by hydrolysis of N_2O_5 on sulfate aerosols could be important for the formation of HNO_3.

$$NO_2 + O_3 \rightarrow NO_3 + O_2 \qquad \text{(R2)}$$

$$NO_2 + NO_3 + M \rightarrow N_2O_5 + M \qquad \text{(R3)}$$

$$N_2O_5 + (H_2O \text{ in sulfate}) \rightarrow 2HNO_3 \qquad \text{(R4)}$$

First, the possible contribution from reaction (R1) is considered. For PEACE-A conditions, the photochemical lifetime of NO_x against reaction (R1), $\overline{\tau_{NO2+OH}}$, is estimated to be 2.5 ± 0.5 days. The diurnally averaged OH concentration (5×10^5 cm^{-3}), the model-predicted NO_2/NO_x ratio (0.7-1.0), and the kinetic parameters recommended by *Sander et al*. [2000] were used for the calculation. The uncertainty in the OH concentration (a factor of 2) was not taken into consideration for the error estimate. Considering the estimated NO_x lifetime of ~1.2 days, reaction (R1) accounts for about half of the NO_x loss rate in the plumes, which suggests that processes other than the reaction of NO_2 + OH were also important for determining the NO_x lifetime during PEACE-A. It should be noted that $\overline{\tau_{NOx}}$ is inversely proportional to the assumed OH concentration as is $\overline{\tau_{NO2+OH}}$ because it is proportional to $\overline{\tau_{C2H4}}$ (equations (7) and (8)). Therefore, the above result (i.e., $\overline{\tau_{NOx}} / \overline{\tau_{NO2+OH}} \sim 0.5$) does not explicitly depend on the uncertainty in the assumed OH concentration.

Second, possible contribution from reactions (R2)-(R4) is considered. Aerosol chemical composition was not measured during PEACE-A. Here we assume that aerosol surface area (A) measured by the Multiple-Angle Aerosol Spectrometer Probe (MASP) [*Liley et al*., 2002] represents the surface area of sulfate aerosols. The surface area in the plumes ranged from 30 to 100 $\mu m^2/cm^3$ (median of 65 $\mu m^2/cm^3$) under cloud-free conditions. Earlier studies showed that the uptake coefficient (γ) for reaction (R4) exhibits large variability, ranging from 0.01 to 0.1 (central value of 0.04) [*Tie et al*., 2003, and references therein]. Using the above numbers as input parameters for the point model, the diurnally averaged NO_x lifetime due to reactions (R2)-(R4) was estimated to be ~1 day for the upper limit case (A = 100 $\mu m^2/cm^3$, $\gamma = 0.1$), ~4 days for the middle case (A = 65 $\mu m^2/cm^3$, $\gamma = 0.04$), and ~30 days for the lower limit case (A = 30 $\mu m^2/cm^3$, $\gamma = 0.01$). These estimates are subject to large uncertainties due to the wide range of γ and the assumption of the sulfate surface area. On the other hand, if we assume that the conditions in the plumes were between the upper limit and middle case, the NO_x loss rate by reactions (R2)-(R4) would be comparable to reaction (R1). Therefore, the NO_x oxidation via reactions (R1)-(R4) can potentially explain most of the NO_x loss processes in the plumes.

Tie et al. [2003] examined the effect of reactions (R2)-(R4) on the NO_x budget, based on a global CTM and the aircraft measurement data obtained during the Tropospheric Ozone Production about the Spring Equinox (TOPSE) mission. They found that this heterogeneous process plays an important role in controlling NO_x concentrations in the Northern Hemispheric mid-to-high latitudes in wintertime. According to their simulations, the NO_x loss rate against reaction (R2), which was the rate-limiting step for reactions (R2)-(R4), was comparable to or even faster than the one against reaction (R1) under similar conditions (altitudes < 3 km, latitudes 25°-40°N, December). Thus, the findings of *Tie et al.* [2003] strongly support the hypothesis in this study.

5.3.2. Interpretation of NO_y lifetime

As mentioned earlier, it was found that only 10-20% of the NO_y compounds emitted from surface sources in East Asia remained in the plumes after 4 days. This fraction is smaller than the NO_y export efficiencies of 20-40% in the boundary layer over the western Pacific during TRACE-P [*Koike et al.*, 2003; *Miyazaki et al.*, 2003], although the relationship between the export efficiencies and air mass aging was not discussed in those studies. *Stohl et al*. [2002] estimated an effective mean NO_y lifetime of 1.7-1.8 days in air masses exported from the United States to the North Atlantic (mainly at 35°-50°N), based on aircraft data obtained during the North Atlantic Regional Experiment in spring 1996 and fall 1997 (NARE 96, 97). The NO_y lifetime estimated in this study (1.7 ± 0.5) is close to the one estimated by *Stohl et al*. It is important to note that both this study and that of *Stohl et al.* estimated NO_y lifetimes of 1-2 days, despite the significant differences in the type of emission sources and meteorological conditions. A common feature found in these two experiments is that a large fraction of NO_y compounds emitted from surface sources were removed within 1-2 days. The transport time of 1-2 days roughly corresponds to the horizontal travel distance of 1000-2000 km in the boundary layer under PEACE-A conditions.

Therefore, this finding suggests that the processing near the source regions is critical in determining the NO_y budget.

6. Summary and Conclusions

Removal of NO_x and NO_y in Asian outflow plumes below 4 km was investigated using aircraft data obtained during the PEACE-A campaign conducted over the western Pacific in January 2002. Correlations of CO with CO_2 and back trajectories were used to identify the plumes transported from source regions in the Asian continent. The plumes originating from Japan (Nagoya) or Korea (Pusan) exhibited relatively low $\Delta CO/\Delta CO_2$ ratios (14-24 ppbv/ppmv), while those from China showed high $\Delta CO/\Delta CO_2$ ratios (28-48 ppbv/ppmv). The observed $\Delta CO/\Delta CO_2$ ratios generally fall within the variability range of the CO/CO_2 emission ratios estimated from the trajectories and the emission inventory based on the work of *Streets et al.* [2003], demonstrating the overall consistency among the aircraft measurements and the emission characterization. The present analysis indicates that $\Delta CO/\Delta CO_2$ ratios can be used as a good tracer for investigating the origins of anthropogenic plumes when the enhancements of CO and CO_2 are large enough and the correlation is tight.

The photochemical age of the plumes was estimated using the observed $\Delta C_2H_4/\Delta C_2H_2$ ratios and the OH concentration calculated by a constrained photochemical box model. Removal of NO_x was investigated using $\Delta NO_x/\Delta CO_2$ ratios and plume age. The photochemical lifetime of NO_x was estimated to be 1.2 ± 0.4 days, which was ~2 times shorter than the lifetime against reaction of NO_2

+ OH. This result suggests that other processes were also important in determining the NO_x lifetime during the PEACE-A period. It is likely that NO_x oxidation by N_2O_5 hydrolysis was another important factor controlling the NO_x lifetime under PEACE-A conditions.

The lifetime of NO_y estimated using $\Delta NO_y/\Delta CO_2$ and plume age was found to be 1.7 ± 0.5 days, indicating the rapid removal of NO_x oxidation products ($NO_z = NO_y - NO_x$) in the plumes. The maximum NO_z yield (i.e., fraction of NO_z produced per NO_x emitted) during the transport was only 10-15%. This maximum appeared at plume ages of 2-3 days, when the NO_x oxidation and NO_z removal rates were likely balanced. The NO_y lifetime obtained in this study was comparable to the NO_y lifetime of 1.7-1.8 days that has previously been reported for outflow from the United States, although there are significant differences in the types of emission sources and meteorological conditions between these two studies. A common feature found in these experiments is that a large fraction of NO_y compounds emitted from surface sources was removed within 1-2 days. This finding suggests the importance of chemical/physical processing (i.e., NO_x oxidation and dry/wet deposition of NO_y) near the source regions in determining the NO_y budget on a regional or even global scale.

Acknowledgments. The authors thank the staff of Diamond Air Service (DAS) for their support and efforts during the aircraft measurements. The PEACE-A mission was supported by the Japan Aerospace Exploration Agency (JAXA) and by the Japanese Ministry of Education, Culture, Sports, Science and Technology (MEXT).

References

Andreae, M. O., B. E. Anderson, D. R. Blake, J. D. Bradshaw, J. E. Collins, G. L. Gregory, G. W. Sachse, and M. C. Shipham, Influence of plumes from biomass burning on atmospheric chemistry over the equatorial and tropical South Atlantic during CITE 3, *J. Geophys. Res*., *99*, 12,793-12,808, 1994.

Atkinson, R., D. L. Baulch, R. A. Cox, R. F. Hampson, Jr., J. A. Kerr, and J. Troe, Evaluated kinetic and photochemical data for atmospheric chemistry supplement IV, *J. Phys. Chem. Ref. Data*, *21*, No.6, 1992.

Blake, N., et al., NMHCs and halocarbons in Asian continental outflow during the Transport and Chemical Evolution over the Pacific (TRACE-P) Field Campaign: Comparison With PEM-West B, *J. Geophys. Res.*, *108*, 8806, doi:10.1029/2002JD003367, 2003.

Calvert, J. G., R. Atkinson, J. A. Kerr, S. Madronich, G. K. Moortgat, T. J. Wallington, and G. Yarwood, The mechanism of atmospheric oxidation of the alkenes, Oxford University Press, 2000.

Hobbs, P. V., P. Sinha, R. J. Yokelson, T. J. Christian, D. R. Blake, S. Gao, T. W. Kirchstetter, T. Novakov, and P. Pilewskie, Evolution of gases and particles from a savanna fire in South Africa, *J. Geophys. Res.*, *108*, 8485, doi:10.1029/2002JD002352, 2003.

Hoell, J. M., D. D. Davis, S. C. Liu, R. Newell, M. Shipham, H. Akimoto, R. J. McNeal, R. J. Bendura, and J. W. Drewry, Pacific Exploratory Mission-West A (PEM-West A): September–October 1991, *J. Geophys. Res.*, 101, 1641– 1653, 1996.

Hoell, J. M., D. D. Davis, S. C. Liu, R. E. Newell, H. Akimoto, R. J. McNeal, and R. J. Bendura, The Pacific Exploratory Mission-West Phase B: February–March, 1994, *J. Geophys. Res.*, 102, 28,223– 28,239, 1997.

Jacob, D. J., J. H. Crawford, M. M. Kleb, V. S. Connors, R. J. Bendura, J. L. Raper, G. W. Sachse, J. C. Gille, L. Emmons, and C. L. Heald, Transport and Chemical Evolution over the Pacific (TRACE-P) aircraft mission: Design, execution, and first results, *J. Geophys. Res.*, *108*, 9000, doi:10.1029/2002JD003276, 2003.

Jaffe, D., H. Price, D. Parrish, A. Goldstein, and J. Harris, Increasing background ozone during spring on the west coast of North America, *Geophys. Res. Lett.*, *30*, 1613, doi:10.1029/2003GL017024, 2003.

Koike, M., et al., Export of anthropogenic reactive nitrogen and sulfur compounds from the East Asia region in spring, *J. Geophys. Res.*, *108*, 8789, doi:10.1029/2002JD003284, 2003.

Kondo, Y., S. Kawakami, M. Koike, D.W. Fahey, H. Nakajima, Y. Zhao , N. Toriyama, M. Kanada, G.W. Sachse, and G.L. Gregory, The performance of an aircraft instrument for the measurement of NO_y, *J. Geophys. Res.*, *102*, 28,663-28,671, 1997.

Kondo, Y., M. Ko, M. Koike, S. Kawakami, and T. Ogawa, Preface to Special Section on Biomass Burning and Lightning Experiment (BIBLE), *J. Geophys. Res.*, *107*, doi:10.1029/2001JD002401, 2002.

Kondo, Y., et al., Impacts of Biomass Burning in Southeast Asia on Ozone and Reactive Nitrogen over the Western Pacific in Spring, *J. Geophys. Res.*, in press, 2004.

Kondo, Y., et al., Photochemistry of ozone over the western Pacific from winter to spring, *J. Geophys. Res.*, this issue.

Liley, J. B., et al., Black carbon in aerosol during BIBLE-B, *J. Geophys. Res.*, *107*, doi:10.1029/2001JD000845, 2002.

Machida, T., K. Kita, Y. Kondo, D. Blake, S. Kawakami, G. Inoue, and T. Ogawa, Vertical and meridional distributions of the atmospheric CO_2 mixing ratio between northern midlatitudes and southern subtropics, *J. Geophys. Res.*, *107*, 8401, doi:10.1029/2001JD000910, 2002.

McKeen, S. A., S. C. Liu, E.-Y. Hsie, X. Lin, J. D. Bradshaw, S. Smyth, G. L. Gregory, and D. R. Blake, Hydrocarbon ratios during PEM-WEST A: A model perspective, *J. Geophys. Res.*, *101,* 2087-2109, 1996.

Miyazaki, Y., et al., Synoptic-scale transport of reactive nitrogen over the western Pacific in spring, *J. Geophys. Res.*, *108*, 8788, doi:10.1029/2002JD003248, 2003.

Nicks Jr, D. K., et al., Fossil-fueled power plants as a source of atmospheric carbon monoxide, *J. Environ. Monit.*, *5*, 35-39, 2003.

Oshima, N., et al., Asian chemical outflow to the Pacific in late spring observed during PEACE-B aircraft campaign, *J. Geophys. Res.*, this issue.

Palmer, P. I., D. J. Jacob, D. B. A. Jones, C. L. Heald, R. M. Yantosca, J. A. Logan, G. W. Sachse, and D. G. Streets, Inverting for emissions of carbon monoxide from Asia using aircraft observations over the western Pacific, *J. Geophys. Res.*, *108*, 8828, doi:10.1029/2003JD003397, 2003.

Sander, S. P., R. R. Friedl, W. B. DeMore, D. M. Golden, M. J. Kurylo, R. F. Hampson, R. E. Huie, G. K. Moortgat, A. R. Ravishankara, C. E. Kolb, and M. J. Molina, Chemical kinetics and photochemical data for use in stratospheric modeling, Evaluation No.13, *JPL Pub*. 2000.

Shirai, T., et al., Emission estimates of selected volatile organic compounds from tropical savanna burning in northern Australia, *J. Geophys. Res.*, *108*, doi:10.1029/2001JD000841, 2003.

Song, C. H., G. Chen, S. R. Hanna, J. Crawford, and D. D. Davis, Dispersion and chemical evolution of ship plumes in the marine boundary layer: Investigation of $O_3/NO_y/HO_x$ chemistry, *J. Geophys. Res.*, *108*, 4143, doi:10.1029/2002JD002216, 2003.

Stohl, A., M. Trainer, T. B. Ryerson, J. S. Holloway, and D. D. Parrish, Export of NO_y from the North American boundary layer during NARE 96 and NARE 97, *J. Geophys. Res.*, *107*, 10.1029/2001JD000519, 2002.

Streets, D. G., et al., An inventory of gaseous and primary aerosol emissions in Asia in the year 2000, *J. Geophys. Res.*, *108*, doi:10.1029/2002JD003093, 2003.

Takegawa, N., et al., Airborne vacuum ultraviolet resonance fluorescence instrument for in situ measurement of CO, *J. Geophys. Res.*, *106*, 24237-24244, 2001.

Takegawa, N., et al., Removal of NO_x and NO_y in biomass burning plumes in the boundary layer over northern Australia, *J. Geophys. Res.*, *108*, doi:10.1029/2002JD002505, 2003.

Tie, X., et al., Effect of sulfate aerosol on tropospheric NO_x and ozone budgets: Model simulations and TOPSE evidence, *J. Geophys. Res.*, *108*, doi:10.1029/2001JD001508, 2003.

Woo, J.-H., et al., Contribution of biomass and biofuel emissions to trace gas distributions in Asia during the TRACE-P experiment, *J. Geophys. Res.*, *108*, 8812, doi:10.1029/2002JD003200, 2003.

Yokelson, R. J., I. T. Bertschi, T. J. Christian, P. V. Hobbs, D. E. Ward, and W. M. Hao, Trace gas measurements in nascent, aged, and cloud-processed smoke from African savanna fires by airborne Fourier transform infrared spectroscopy (AFTIR), *J. Geophys. Res.*, *108*, 8478, doi:10.1029/2002JD002322, 2003.

Zhang, J., K.R. Smith, Y. Ma, S. Ye, F. Jiang, W. Qi, P. Liu, M.A.K. Khalil, R.A. Rasmussen, and S.A. Thorneloe, Greenhouse gases and other airborne pollutants from household stoves in China: a database for emission factors *Atmos. Environ.*, *34*, 4537-4549, 2000.

Figure captions

Figure 1. Flight tracks of the Gulfstream-II (G-II) aircraft during the Pacific Exploration of Asian Continental Emission Phase A (PEACE-A) campaign.

Figure 2. Vertical profiles of (a) CO (solid) and CO_2 (shaded); (b) NO_y (solid) and NO_x (shaded); and (c) O_3 (solid) and relative humidity (RH) (shaded) observed over the Sea of Japan (132°E, 36°N) on January 11, 2002 (flight 04).

Figure 3. 1° x 1° grid distribution of CO/CO_2 emission ratios for January 2002. The color code represents the CO/CO_2 emission ratios, and the size of the symbols represents the CO emission rate (Gmol $month^{-1}$ $grid^{-1}$). Rectangular sections represent the source regions defined in Table 1.

Figure 4. Correlation of CO with CO_2 for the plumes listed in Table 2. The data are 1-s averages. Black, red, and blue dots represent the Japan, Korea, and China plumes, respectively (Table 2). The China plumes include both Northern and Central China plumes. The

dashed lines represent the variability range of the CO/CO_2 emission ratios in the individual source regions estimated from the emission inventory.

Figure 5. (a) Time series of CO mixing ratio (solid lines and shaded line) and aircraft cruise altitude (dashed line) observed off Korea on January 7, 2002. The air masses indicated by the solid line correspond to the Korea-1 (F02L08) plume in Table 2. The air masses indicated by the horizontal arrow were excluded because they were transported from Central China without having passed over Korea. (b) and (c) Back trajectories for the plume. (d) Correlation of CO and CO_2 in the plume (solid circles). Solid line represents the linear regression for the data. Doted-dashed line and two dashed lines represent the average, maximum, and minimum values of the CO/CO_2 emission ratio from the Korea region, respectively.

Figure 6. Same as Figure 5 but for a plume transported from Northern China observed on January 11, 2002. These air masses correspond to the N-China-1 (F04L02) plume in Table 2.

Figure 7. Correlations of (a) methyl bromide (CH_3Br) and (b) Halon-1211 (H-1211) with CO in the Korea-1 (F02L08) plume (same plume as used in Figure 5). Solid lines are linear regression lines, and the dashed line is taken from *Blake et al.* [2003].

Figure 8. Same as Figure 7 but for the N-China-1 (F04L02) plume (same plume as used in Figure 6).

Figure 9. Correlations of (a) NO_y with CO and (b) NO_y with CO_2 observed below 1.6 km over Nagoya, Japan. Solid circles and shaded circles represent the Japan-2 (F02L14) and the Japan-4 (F03L08) plumes, respectively. Solid and shaded lines represent the regression

lines. Emission ratios estimated from the emission inventory (doted-dashed line: average; dashed lines: maximum and minimum) are also shown.

Figure 10. Correlations of (a) NO_x and (b) NO_y with CO_2 in the Korea-1 (F02L08) plume (same plume as used in Figure 5). Solid lines are linear regression lines. Doted-dashed line and two dashed lines represent the average, maximum, and minimum values of the NO_x/CO_2 emission ratio from the Korea region, respectively

Figure 11. Same as Figure 10 but for the N-China-1 (F04L02) plume (same plume as used in Figure 6).

Figure 12. (a) $(\Delta NO_x/\Delta CO_2)/E_{NOx\text{-}CO2}$ and (b) $(\Delta NO_y/\Delta CO_2)/E_{NOx\text{-}CO2}$ as a function of plume age defined by equation (7). Data points are colored based on average sampling altitudes. Solid curves were determined by a least squares fit to the data. The error bars were determined from fitting errors for the NO_x-CO_2 (or NO_y-CO_2) correlations and the maximum and minimum values of the NO_x to CO_2 emission ratios.

Figure 13. (a) Average NO_x/NO_y ratio and (b) $(\Delta NO_z/\Delta CO_2)/E_{NOx\text{-}CO2}$ as a function of plume age, where NO_z (= $NO_y - NO_x$) represents the NO_x oxidation products. The error bars for the NO_x/NO_y ratios represent 1-σ of the average. The error bars for the $(\Delta NO_z/\Delta CO_2)/E_{NOx\text{-}CO2}$ were determined from fitting errors for the NO_z-CO_2 correlations and the maximum and minimum values of the NO_x to CO_2 emission ratios.

Author address

D. R. Blake, Department of Chemistry, University of California, Irvine, Irvine CA 92697-2025, USA. (dblake@uci.edu)

G. R. Carmichael, J.-H. Woo, Center for Global and Regional Environmental Research, University of Iowa, Iowa, IA 52242, USA. (gcarmich@engineering.uiowa.edu, woojh21@cgrer.uiowa.edu)

G. Chen, NASA Langley Research Center, Hampton, VA 23681-0001 USA. (g.chen@larc.nasa.gov)

K. Kita, Department of Environmental Sciences, Faculty of Science, Ibaraki University, 2-1-1 Bunkyo, Mito, Ibaraki 310-8512, Japan. (kita@env.sci.ibaraki.ac.jp)

M. Koike, Department of Earth and Planetary Science, Graduate School of Science, University of Tokyo, 7-3-1 Hongo, Bunkyo-ku, Tokyo 113-0033, Japan. (koike@eps.s.u-tokyo.ac.jp)

Y. Kondo, Y. Miyazaki, and N. Takegawa, Research Center for Advanced Science and Technology, University of Tokyo, 4-6-1 Komaba, Tokyo 153-8904, Japan. (kondo@atmos.rcast.u-tokyo.ac.jp, yuzom@atmos.rcast.u-tokyo.ac.jp, takegawa@atmos.rcast.u-tokyo.ac.jp)

J. B. Liley, National Institute of Water and Atmospheric Research, Private Bag 50061, Omakau, Central Otago, New Zealand (b.liley@niwa.co.nz)

T. Machida, National Institute for Environmental Studies, Tsukuba 305-0053, Japan. (tmachida@nies.go.jp)

T. Shirai, and T. Ogawa, Earth Observation Research and Application Center, Japan Aerospace Exploration Agency, 1-8-10 Harumi, Tokyo 104-6023, Japan. (shirai@eorc.jaxa.jp, ogawa.toshihiro@jaxa.jp)

D. G. Streets, Decision and Information Sciences Division, Argonne National Laboratory, Argonne, IL 60439, USA. (dstreets@anl.gov)

T. Watai, Global Environmental Forum, Tsukuba 305-0053, Japan. (watai.tomonori@nies.go.jp)

Table 1. Emission Ratios of Trace Gases for Individual Source Regions [a]

Source region	Longitude, Latitude	CO/CO_2, 10^{-3} mol/mol	NO_x/CO, mol/mol	NO_x/CO_2, 10^{-3} mol/mol	C_2H_4/C_2H_2, mol/mol
Japan (Nagoya)	136°-138°E, 34°-36°N	9 (7-14)	0.21 (0.18-0.23)	1.8 (1.5-2.5)	2.0 (1.9-2.3)
Korea (Pusan)	126°-130°E, 34°-36°N	19 (16-22)	0.22 (0.20-0.23)	4.1 (3.8-4.3)	2.1 (2.0-2.2)
Northern China	110°-125°E, 35°-44°N	52 (30-104)	0.044 (0.022-0.079)	2.3 (1.2-3.3)	1.7 (1.3-3.2)
Central China	105°-123°E, 26°-35°N	56 (38-96)	0.032 (0.013-0.067)	1.8 (0.9-3.8)	1.7 (1.6-2.4)

[a] Average of emission ratios derived from the emission inventory for January 2002. The values in parentheses represent the minimum and maximum values of the emission ratios.

Table 2. Plume Identification

Plume ID [a]			Sampling location			Number of	r^2 for CO-CO_2	$\Delta CO/\Delta CO_2$,
Group	Flight No.	Leg No.	Longitude, °E	Latitude, °N	Altitude, km	1-s data points	correlation	ppbv/ppmv [b]
				Japan plumes				
Japan-1	F02	L02	135.8-136.1	36.3-36.4	0.7-2.5	230	0.89	17 (± 0.4)
Japan-2	F02	L14	136.9-137.0	35.0-35.2	0.4-1.0	209	0.99	18 (± 0.1)
Japan-3	F03	L02	139.4-139.9	32.5-34.2	0.2-1.8	1708	0.79	16 (± 0.2)
Japan-4	F03	L08	137.0-137.2	35.0-35.1	0.8-1.6	311	0.99	14 (± 0.1)
				Korea plumes				
Korea-1	F02	L08	129.6-131.1	34.9-35.7	0.2-2.0	1302	0.98	24 (± 0.1)
	F02	L12	128.7-129.7	33.8-34.9	0.2-1.4	1137	0.88	22 (± 0.2)
				Northern China plumes				
N-China-1	F04	L02	133.3-136.0	35.9-36.3	0.2-3.9	1867	0.97	38 (± 0.2)
	F04	L04	132.0-134.9	35.7-36.6	0.2-3.0	1917	0.98	36 (± 0.1)
N-China-2	F04	L06	136.2-136.6	37.3-37.4	1.0-3.0	240	0.99	35 (± 0.3)
	F05	L05	138.1-138.4	39.2-40.2	1.8-4.0	687	0.79	28 (± 0.5)
N-China-3	F06	L01	136.9-137.0	35.3-35.4	1.0-2.9	65	0.95	35 (± 1)
	F06	L03	135.8-136.2	36.3-36.4	1.6-4.0	255	0.98	40 (± 0.4)
				Central China plumes				
C-China-1	F07	L02	128.3-128.4	30.1-30.1	1.3-2.0	66	0.99	48 (± 0.3)
	F07	L09	127.6-128.0	29.8-30.0	1.3-4.0	282	0.96	43 (± 0.5)
C-China-2	F07	L05	124.9-125.0	27.5-27.9	1.2-4.0	270	0.94	28 (± 0.5)
	F07	L07	125.9-126.1	29.0-29.2	1.2-4.0	280	0.77	29 (± 1)
C-China-3	F07	L10	130.0-130.8	31.3-31.6	1.3-4.0	910	0.88	36 (± 0.4)
C-China-4	F12	L05	130.6-130.9	31.3-31.8	2.0-3.0	1069	0.99	42 (± 0.1)

Caption for Table 2

[a] Each plume ID consists of a group name, flight number, and leg number. The duration of individual flights (F01, F02, etc.) were divided into 5-14 flight legs (L01, L02, etc.) based on back trajectories. The name of each group represents the source region (defined in Table 1) estimated from the trajectories. Different flight legs with similar sampling locations on the same day were categorized as the same group.

[b] $\Delta CO/\Delta CO_2$ ratios were determined from linear regression analysis.

Table 3. Photochemical Lifetime of CO and NMHCs under the Conditions Experienced during PEACE-A

Species	Lifetime, day [a]
CO	100
Ethane (C_2H_6)	120
Ethene (C_2H_4)	2.7
Ethyne (C_2H_2)	35
Propane (C_3H_8)	24
Propene (C_3H_6)	0.8

[a] Median value of the diurnally averaged OH concentration of 5×10^5 cm^{-3} (< 3 km, 25°-45°N) was used for the calculation.

Table 4. Plume Age and Lifetimes of NO_x and NO_y for Individual Plumes

Plume ID		Plume age,	Transport	NO_x		NO_y	
Group	Flight & leg No.	day [a]	time, day [b]	$(\Delta NO_x/\Delta CO_2)/E_{NOx\text{-}CO2}$	τ_{NOx}, day	$(\Delta NO_y/\Delta CO_2)/E_{NOx\text{-}CO2}$	τ_{NOy}, day
Japan-1	F02L02	3.0 (+0.3/-0.1)	< 1	0.09 (+0.02/-0.03)	1.2 (+0.3/-0.2)	0.19 (+0.04/-0.06)	1.8 (+0.4/-0.4)
Japan-3	F03L02	2.2 (+1.1/-0.8)	< 1	0.35 (+0.12/-0.20)	2.1 (+2.2/-1.3)	0.44 (+0.14/-0.24)	2.6 (+3.4/-1.8)
Korea-1	F02L08	1.8 (+0.4/-0.3)	< 1	0.15 (+0.01/-0.01)	0.9 (+0.3/-0.2)	0.17 (+0.02/-0.01)	1.0 (+0.3/-0.2)
N-China-1	F04L02	3.1 (+1.9/-0.9)	1-2	0.05 (+0.05/-0.02)	1.0 (+1.1/-0.4)	0.16 (+0.15/-0.05)	1.7 (+2.6/-0.7)
	F04L04	2.3 (+1.9/-0.8)	1-2	0.06 (+0.05/-0.02)	0.8 (+1.1/-0.4)	0.17 (+0.16/-0.06)	1.3 (+2.5/-0.6)
C-China-2	F07L05	4.3 (+0.9/-0.3)	1-3	0.02 (+0.02/-0.01)	1.1 (+0.6/-0.2)	0.03 (+0.04/-0.02)	1.3 (+0.8/-0.3)
	F07L07	4.0 (+1.0/-0.3)	1-3	0.008 (+0.01/-0.004)	0.8 (+0.4/-0.2)	0.06 (+0.08/-0.03)	1.5 (+1.1/-0.4)
C-China-3	F07L10	3.8 (+0.9/-0.3)	1-3	0.06 (+0.07/-0.03)	1.4 (+1.0/-0.4)	0.14 (+0.17/-0.08)	2.0 (+2.0/-0.7)

[a] Plume age was derived from $\Delta C_2H_4/\Delta C_2H_2$ ratios ([OH] = 5 x 10^5 cm^{-3}).

[b] Transport time was roughly estimated based on trajectories.

Figure 1

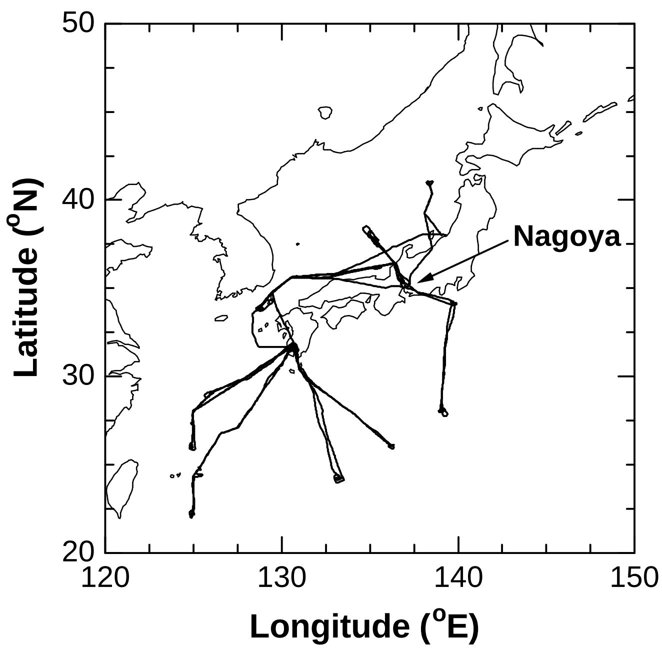

Figure 2

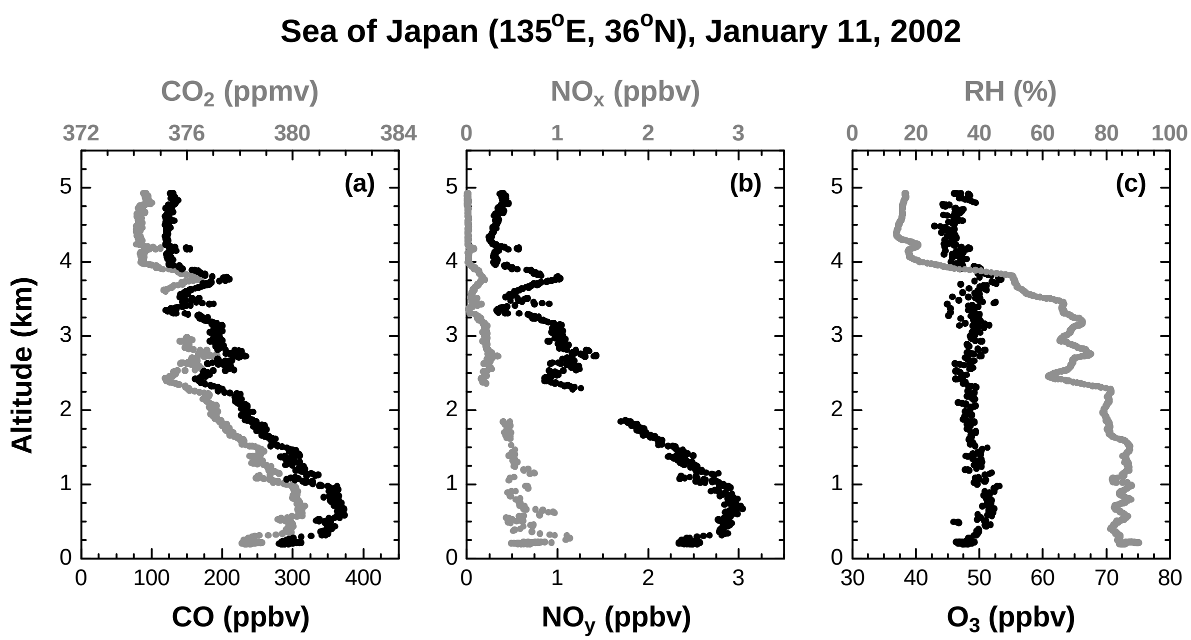

Figure 3

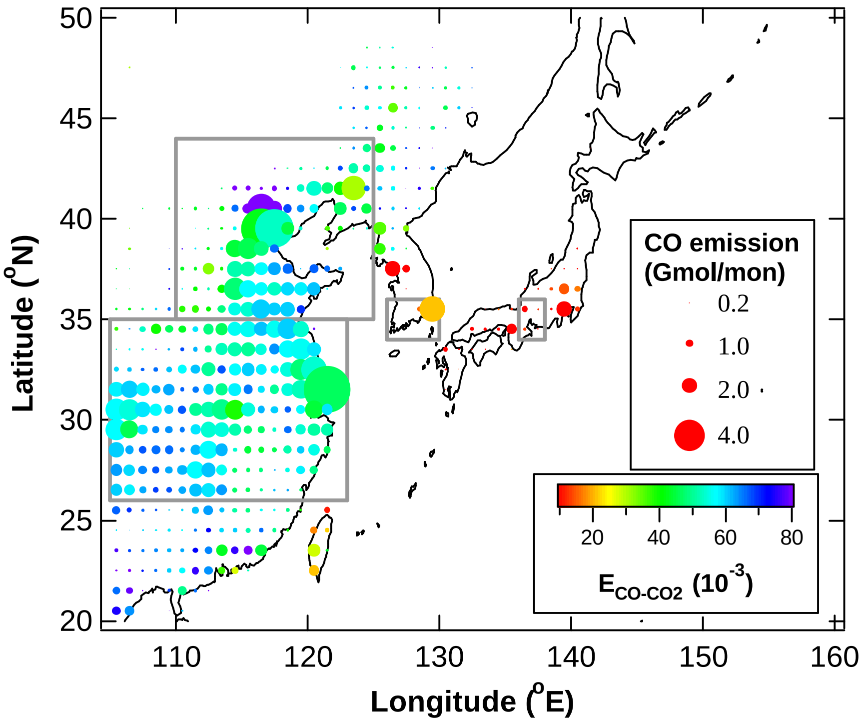

50
45
40
35
30
25
20
110
120
130
140
150
160
Latitude (°N)
Longitude (°E)
CO emission
(Gmol/mon)
0.2
1.0
2.0
4.0
20
40
60
80
E_CO-CO2 (10^-3)

Figure 4

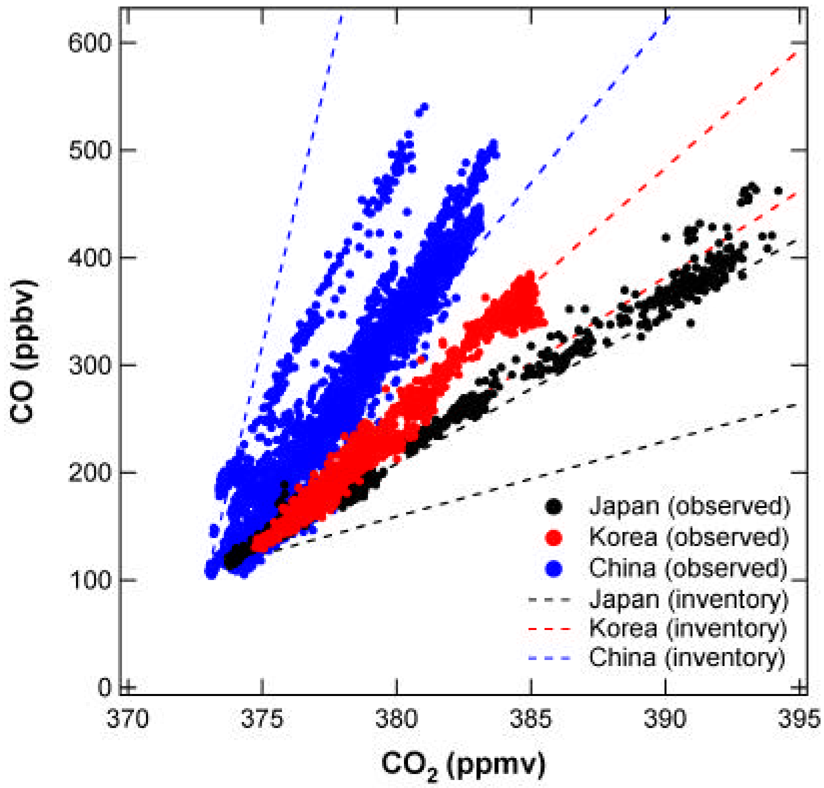

CO (ppbv)
600
500
400
300
200
100
0
370
375
380
385
390
395
CO_2 (ppmv)
Japan (observed)
Korea (observed)
China (observed)
Japan (inventory)
Korea (inventory)
China (inventory)

Figure 5

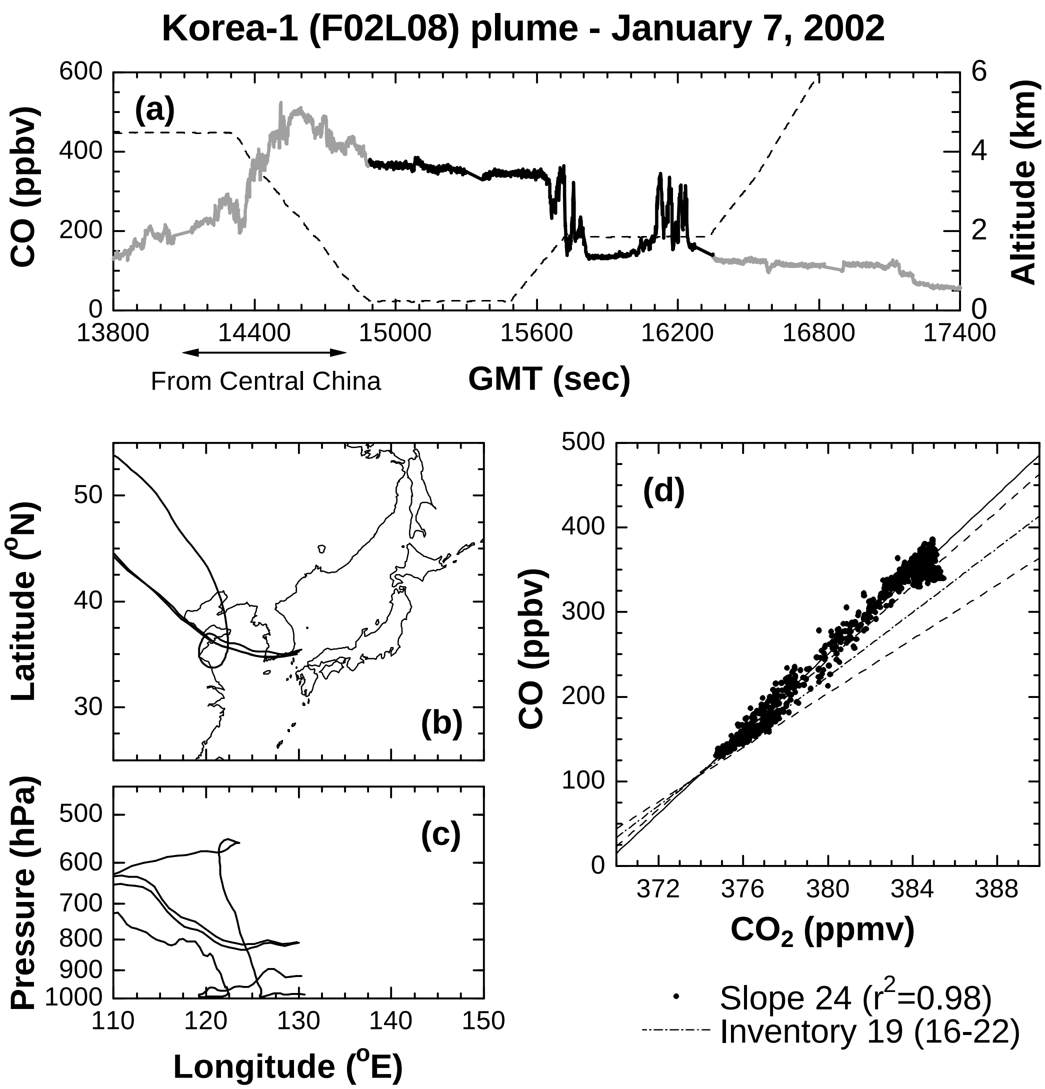
Korea-1 (F02L08) plume - January 7, 2002
(a)
CO (ppbv)
Altitude (km)
600
400
200
0
6
4
2
0
13800
14400
15000
15600
16200
16800
17400
From Central China
GMT (sec)
(b)
Latitude (oN)
50
40
30
(c)
Pressure (hPa)
500
600
700
800
900
1000
110
120
130
140
150
Longitude (oE)
(d)
CO (ppbv)
500
400
300
200
100
0
372
376
380
384
388
CO2 (ppmv)
Slope 24 (r2=0.98)
Inventory 19 (16-22)

Figure 6

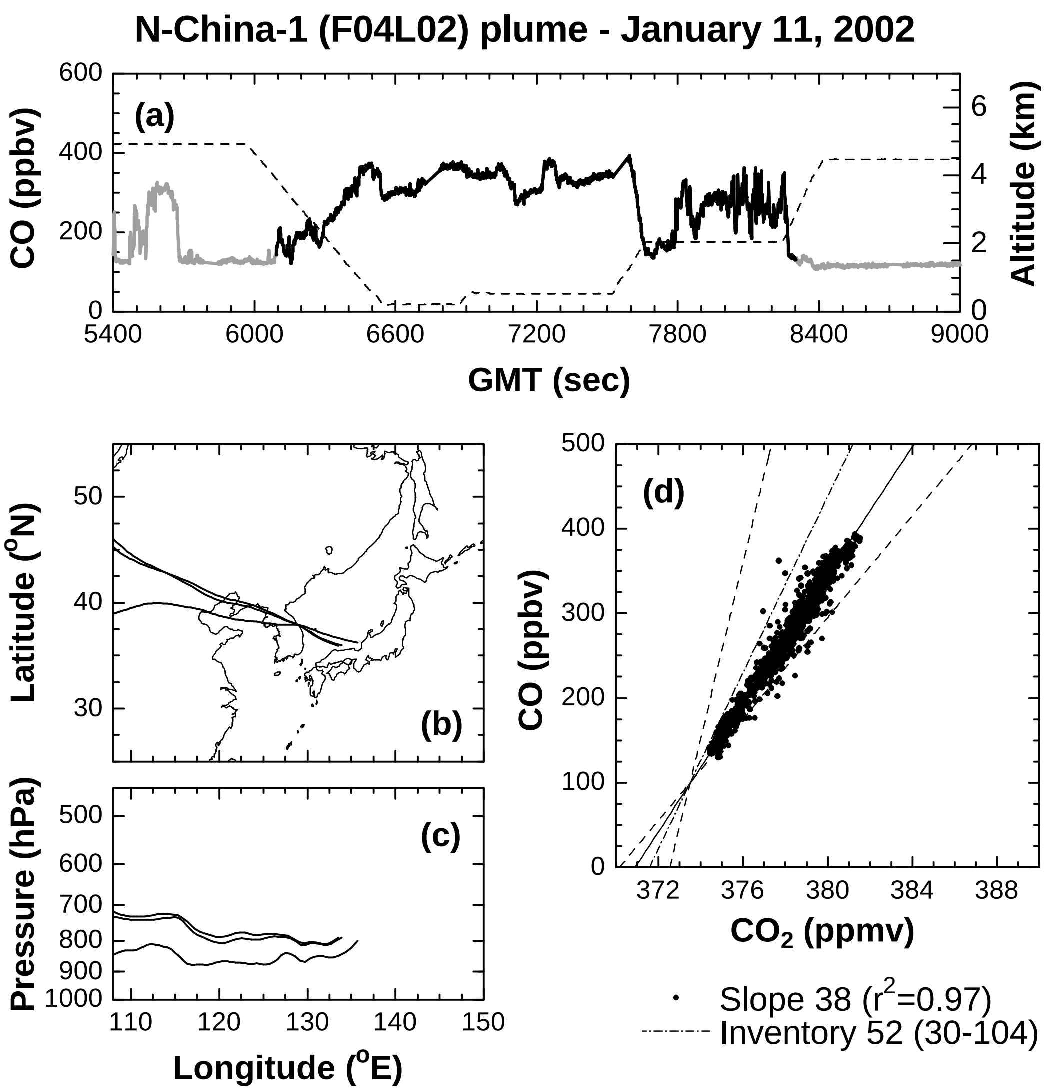

N-China-1 (F04L02) plume - January 11, 2002
(a)
CO (ppbv)
Altitude (km)
GMT (sec)
5400
6000
6600
7200
7800
8400
9000
0
200
400
600
0
2
4
6
(b)
Latitude (oN)
50
40
30
(c)
Pressure (hPa)
500
600
700
800
900
1000
110
120
130
140
150
Longitude (oE)
(d)
CO (ppbv)
0
100
200
300
400
500
372
376
380
384
388
CO2 (ppmv)
Slope 38 (r2=0.97)
Inventory 52 (30-104)

Figure 7

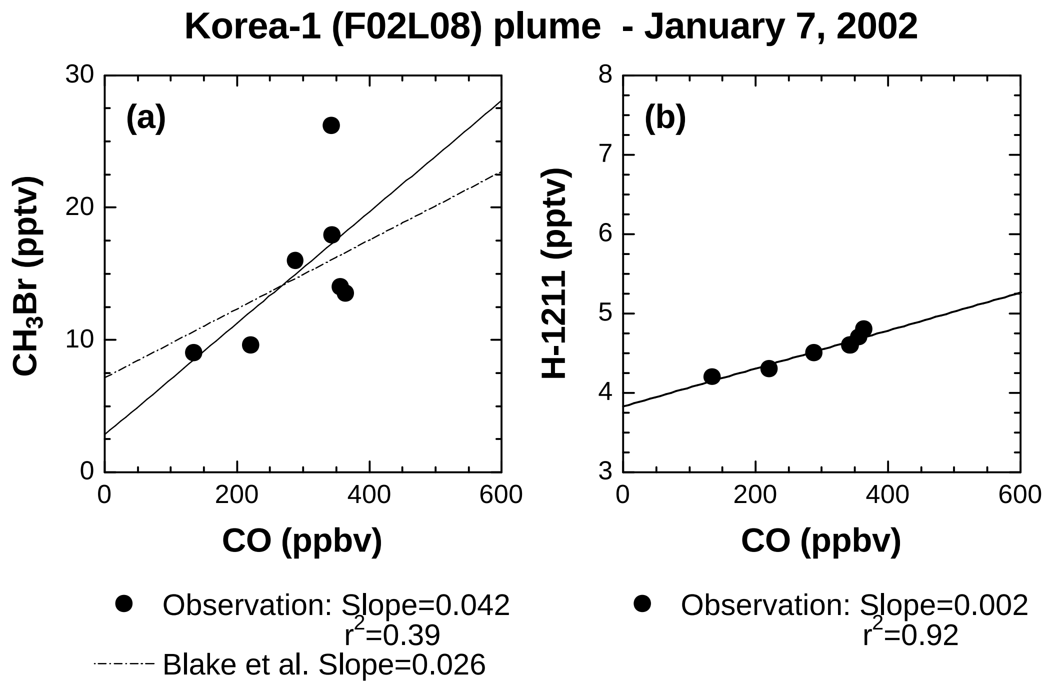

Figure 8

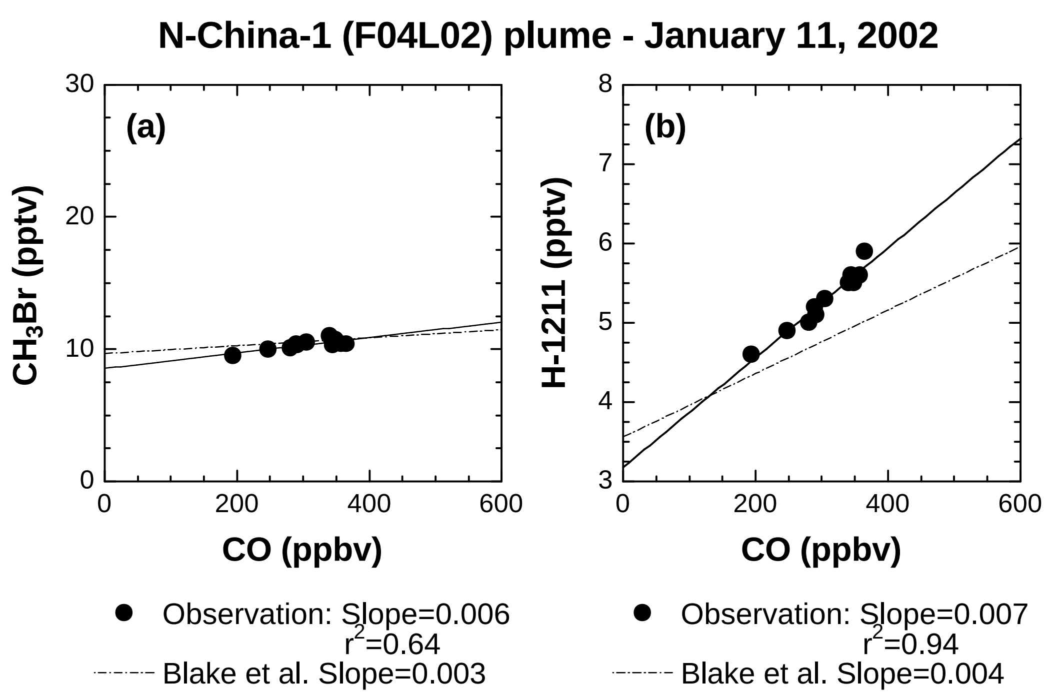

Figure 9

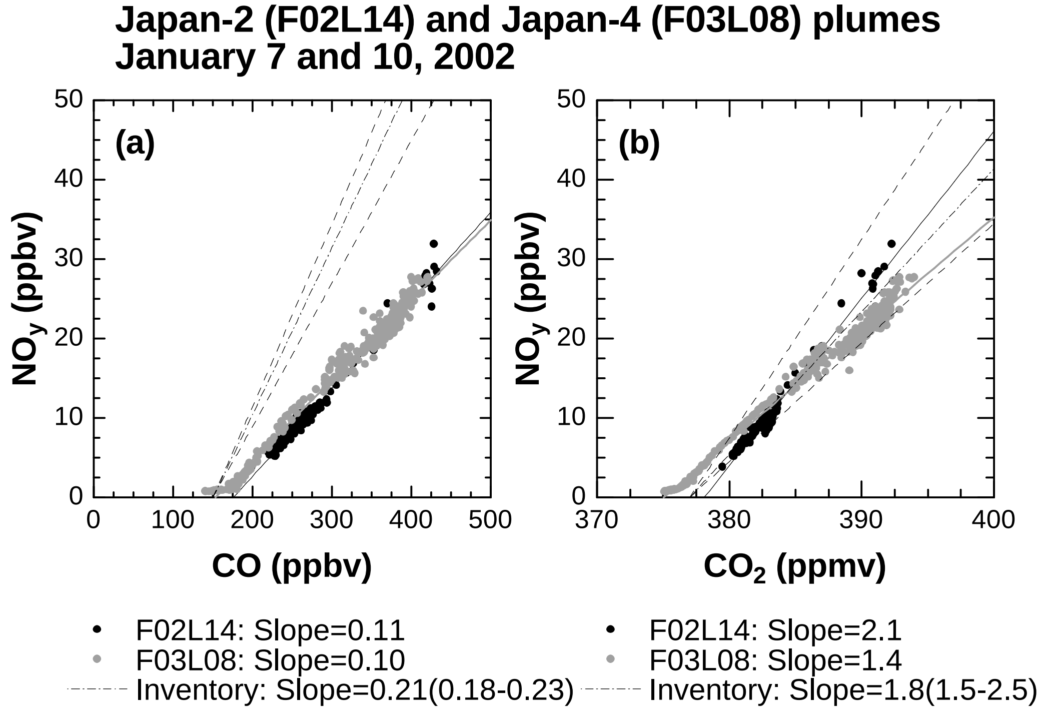

Japan-2 (F02L14) and Japan-4 (F03L08) plumes
January 7 and 10, 2002
(a)
(b)
NOy (ppbv)
CO (ppbv)
CO2 (ppmv)
0
10
20
30
40
50
0
100
200
300
400
500
370
380
390
400
F02L14: Slope=0.11
F03L08: Slope=0.10
Inventory: Slope=0.21(0.18-0.23)
F02L14: Slope=2.1
F03L08: Slope=1.4
Inventory: Slope=1.8(1.5-2.5)

Figure 10

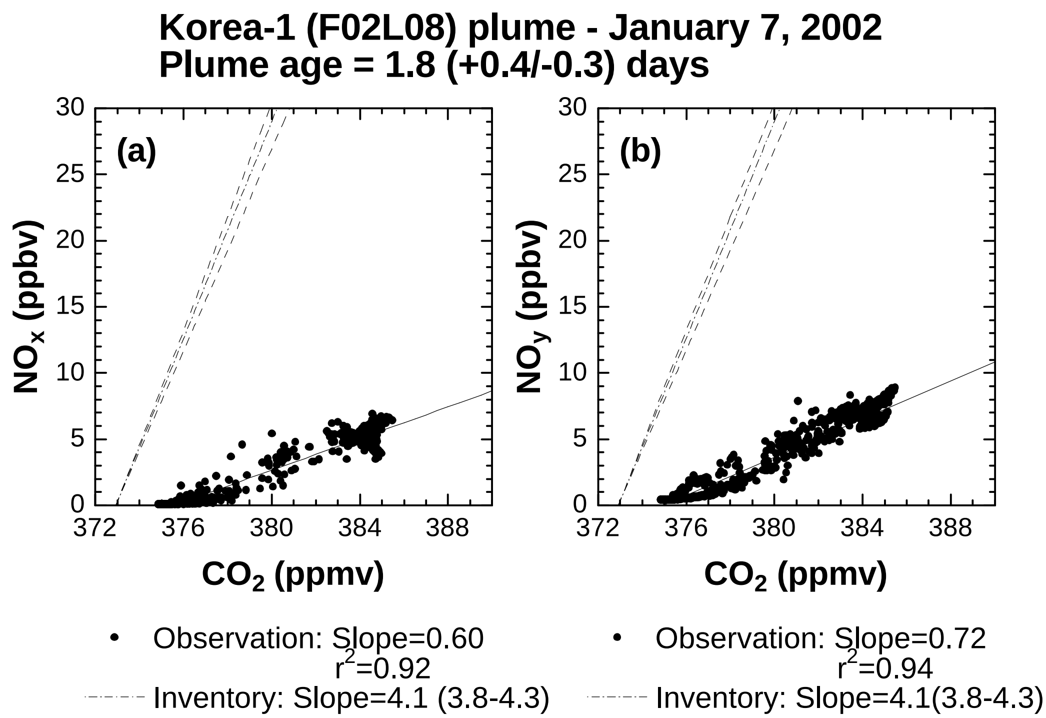

Figure 11

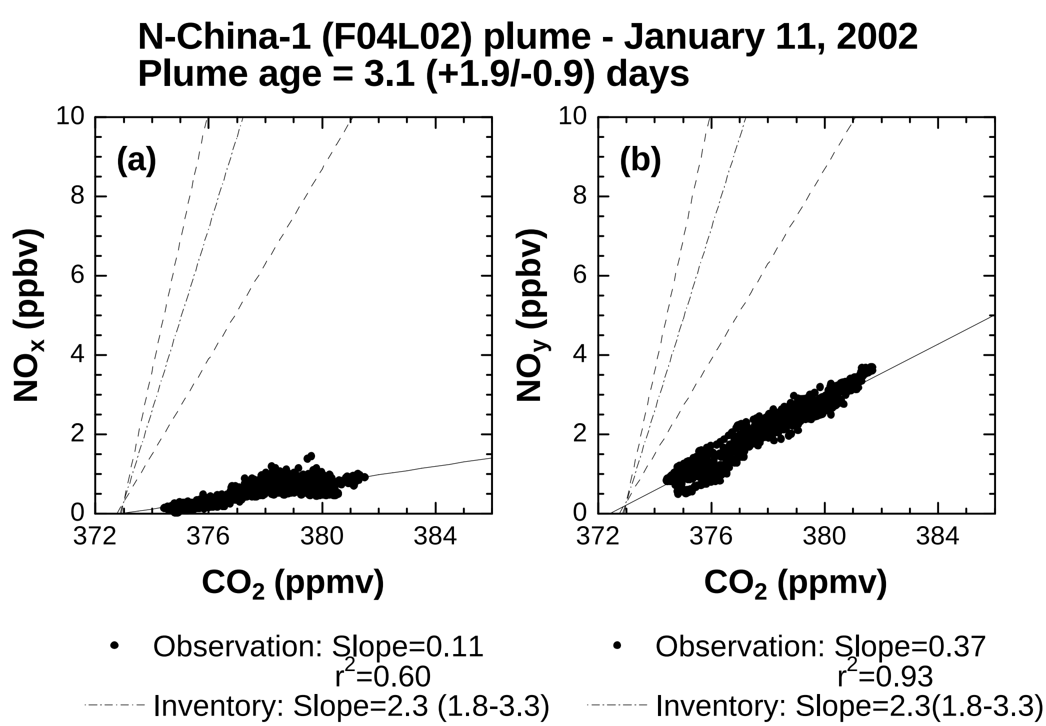

Figure 12

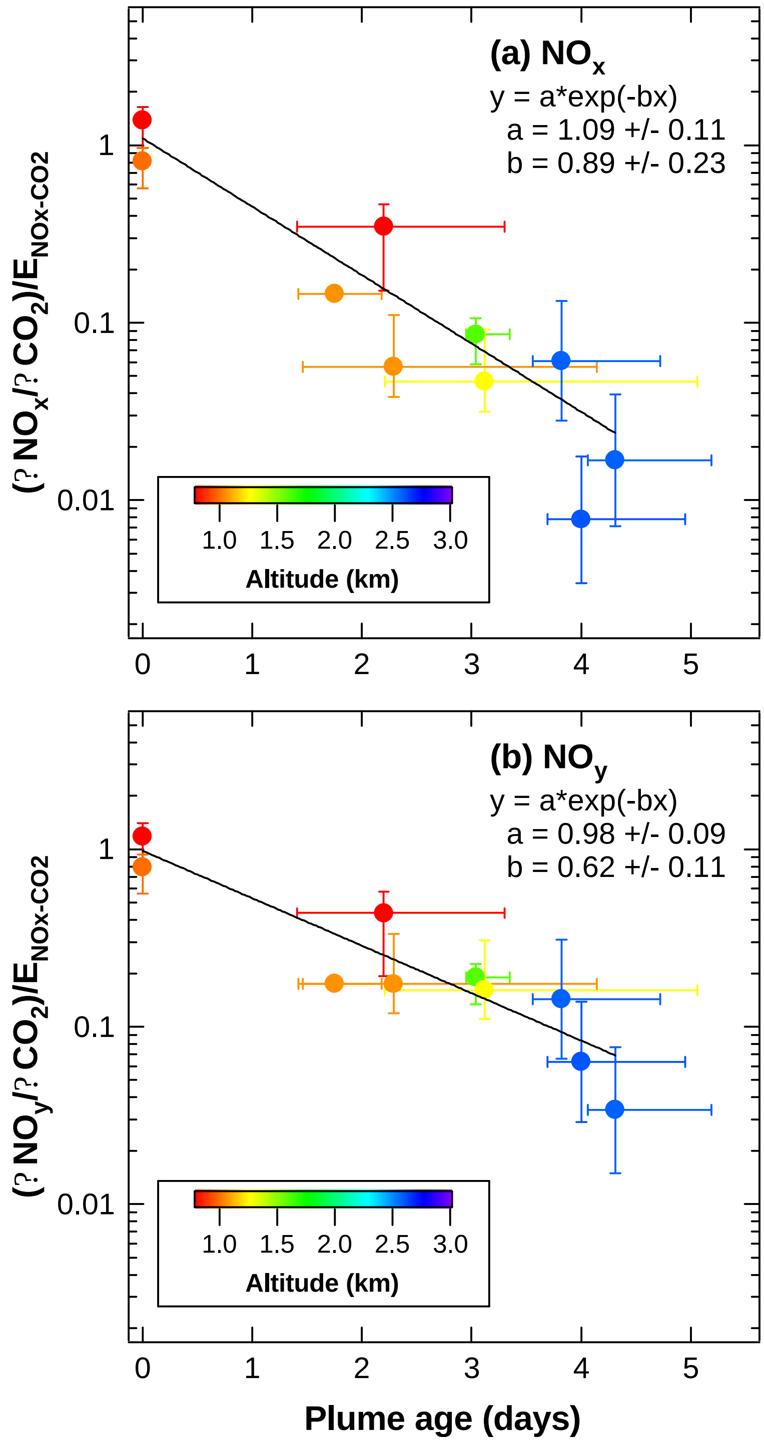

(a) NOx
y = a*exp(-bx)
a = 1.09 +/- 0.11
b = 0.89 +/- 0.23
(? NOx/? CO2)/ENOx-CO2
1
0.1
0.01
1.0 1.5 2.0 2.5 3.0
Altitude (km)
0 1 2 3 4 5
(b) NOy
y = a*exp(-bx)
a = 0.98 +/- 0.09
b = 0.62 +/- 0.11
(? NOy/? CO2)/ENOx-CO2
1
0.1
0.01
1.0 1.5 2.0 2.5 3.0
Altitude (km)
0 1 2 3 4 5
Plume age (days)

Figure 13

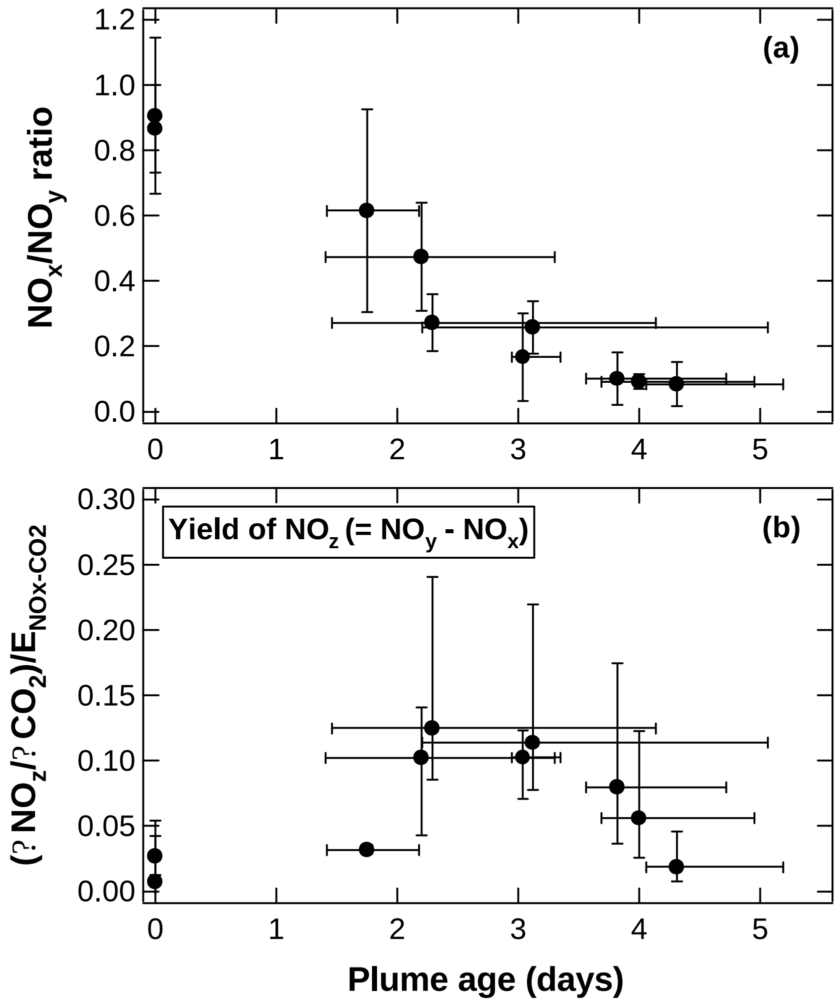

(a)
NOx/NOy ratio
1.2
1.0
0.8
0.6
0.4
0.2
0.0
0 1 2 3 4 5
(b)
Yield of NOz (= NOy - NOx)
(? NOz/? CO2)/ENOx-CO2
0.30
0.25
0.20
0.15
0.10
0.05
0.00
0 1 2 3 4 5
Plume age (days)